P6.162 Single and Dual-Doppler Radar Observations of a Nontornadic Supercell Thunderstorm on 6 June 2010

ZACHARY WIENHOFF AND JEFFREY FRAME

Department of Atmospheric Sciences, University of Illinois at Urbana-Champaign, Urbana, IL

1. Introduction

Two Doppler on Wheels (DOW) radars (Wurman et al. 1997) intercepted a nontornadic supercell near Ogallala, Nebraska, on 6 June 2010 during the Verification of the Origins of Rotation in Tornadoes Experiment 2 (Wurman et al. 2012). The storm initiated within a disorganized cluster of convection north of Sydney, Nebraska, at approximately 2000 UTC in a region of moist upslope flow east of a lee surface trough (Fig. 1a). The 0-6 km bulk shear was approximately 60 knots (Fig. 1b), which was more than sufficient for organized convection, including supercells. As the storm progressed eastward and low-level wind fields strengthened, the storm entered a region with 0-1 km storm-relative helicity (SRH) of approximately 200 m^2 s^{-2} (Fig. 1c). Within this regime, the easternmost cell organized into a right-moving supercell around 2200 UTC.

Mobile Doppler radar observations began at approximately 2245 UTC, while the storm was a mature right-moving supercell and lasted for approximately 90 minutes, by which time the storm had weakened significantly. Herein, only single-Doppler analyses are used to examine the cell, given the paucity of potential dual-Doppler analysis volume scans (only twelve minutes of such data exist).

This storm is of interest because the close proximity of the radars to the storm (less than 15 km) allows for relatively high-resolution objective analyses of reflectivity and radial velocity fields near the mesocyclone. While detailed analyses of one of the strong tornadoes intercepted by VORTEX2 is well underway (e.g., Wakimoto et al. 2011; Markowski et al. 2012a, b; Atkins et al. 2012; Kosiba et al. 2012), detailed examinations of nontornadic supercells (e.g., Trapp 1999; Wakimoto and Kai 2000; Beck et al. 2006; Frame et al. 2009) are equally important in determining potentially significant differences between tornadic and nontornadic supercells.

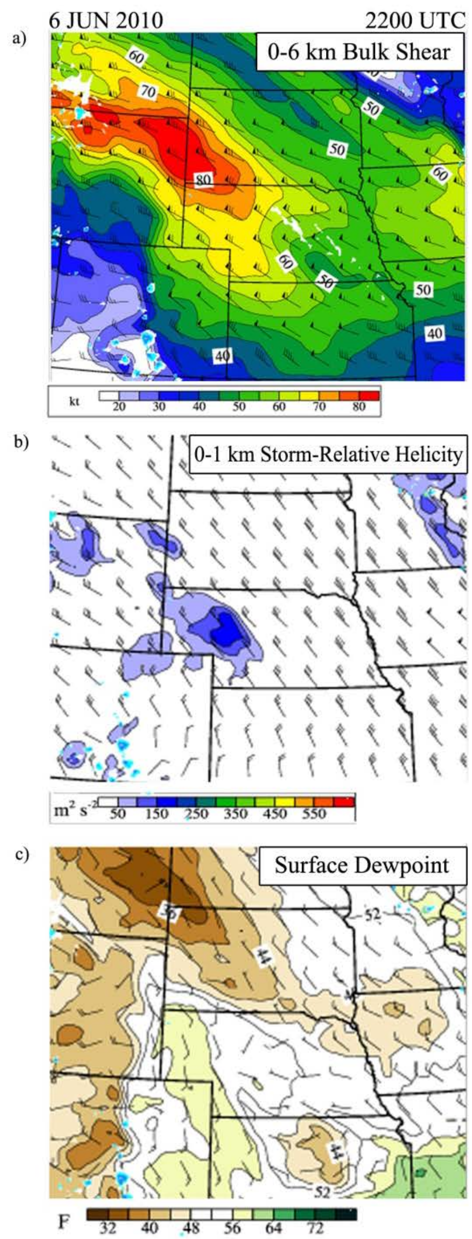

FIG. 1. 22-hour NSSL WRF forecast initialized at 0000 UTC 6 June 2010 for the northern Great Plains. Included products are (a) 0-6 km bulk shear (knots), (b) 0-1 km storm-relative helicity (SRH; m^2 s^{-2}), and (c) surface dewpoint temperatures (˚F) and wind barbs (knots).

The primary focus of this paper is to document the temporal evolution of the rear-flank downdraft (RFD), rear-flank gust front, and mesocyclone, and to draw preliminary conclusions as to why the storm failed to produce a tornado during the time in which it was observed by the radars. A brief overview of the data and methodology can be found in section 2. Section 3 presents the radar observations, and preliminary conclusions and future work are listed in section 4.

2. Data and Methodology

Data from two mobile Doppler radars (DOW6 and DOW7) are presented after being edited for quality using SOLOII software (Oye et al 1995). The radars were originally located 25 km south of Ogallala, NE, before relocating southeast to follow the supercell (Fig. 2). The radars are dual-polarization X-band (3 cm wavelength) radars and have a beamwidth of 0.95˚. Volume scans were completed simultaneously every two minutes and included elevation angles of 0.5˚, 1˚, 2˚, 3˚, 4˚, 5˚, 6˚, 8˚, 10˚, 12˚, and 14˚. Quality control included removing data with poor signal-to-noise ratios, deleting second trip echoes, and dealiasing folded velocities. These data were then mapped to a Cartesian grid using REORDER software (Oye and Case 1992) and a one-pass Barnes analysis (Barnes 1964). The Cartesian grid dimensions are 30 × 20 × 3 km, and the horizontal and vertical grid spacing is 100 m. A smoothing parameter of $\kappa = 0.102$ km^2 was used and data beyond 720 m from a grid point did not contribute to the analysis at that grid point. The above objective analysis parameters are consistent with the recommendations given by Pauley and Wu (1990) and Marquis et al. (2007).

3. Observations

When mobile Doppler radar observations began around 2245 UTC, the storm had developed a hook echo and displayed a "flying eagle" signature, with a V-shaped notch within the forward-flank reflectivity core (e.g., van den Brocke et al. 2008; Kumjian and Schenkman 2008; Frame et al. 2009). The maximum reflectivity within the core was approximately 75 dBZ as per WSR-88D imagery (Figs. 3a and 3b). The storm began to lose organization around 2339 UTC (Fig. 3c) and reflectivities within the core began to decrease. After this time, VORTEX2 abandoned this storm in favor of another storm farther to the north, which is not discussed in this paper.

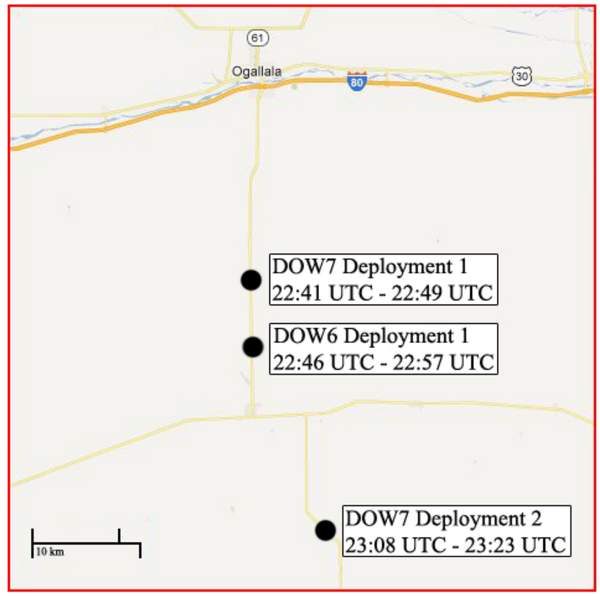

FIG. 2. Map of the DOW deployment sites. Corresponding observation times are shown.

At the beginning of the mobile radar observation period, east-southeasterly winds ranging from 8 to 16 m s^{-1} existed within the storm inflow southeast of the cell and persisted throughout the scanning period. A prominent hook echo is visible in the first volume scan from DOW7 (Fig. 4a) at 2245 UTC. In the DOW data, the storm displayed a maximum reflectivity of around 55 dBZ near the hook echo. The DOW reflectivity values are different from those in the WSR-88D imagery because of the different wavelengths and calibrations used between the radars. The left-forward flank of the storm is not visible on the DOW imagery because the DOW radar beam was attenuated within the forward flank of the storm owing to heavy rain and hail there; the 3 cm wavelength beam used by the DOW experiences significantly more attenuation as compared to the 10 cm wavelength used by the WSR-88D radars (Doviak and Zrnic 1993, p. 42). Also at this time, a weak "donut hole," approximately 1.25 km in diameter, is visible about 900 m above the surface, coincident with weak rotation at this level (not shown).

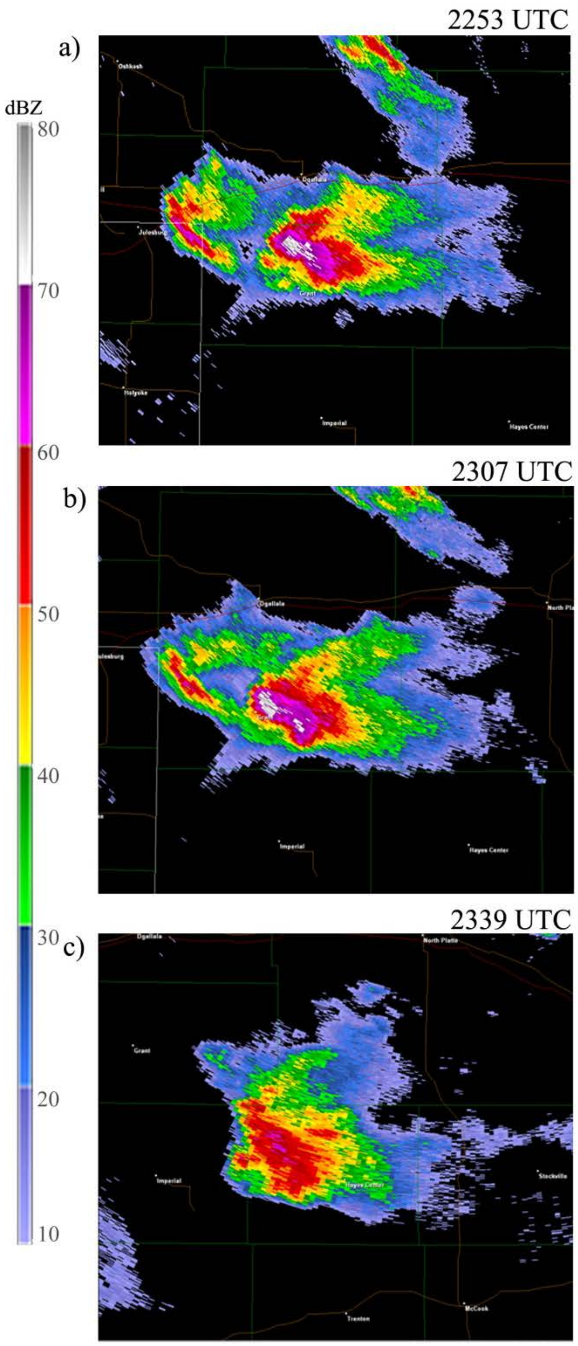

FIG. 3. KLNX WSR-88D radar reflectivity at (a) 2253 UTC, (b) 2307 UTC, and (c) 2339 UTC 6 June 2010.

A line of enhanced reflectivities, which connects to the forward flank precipitation core about 5 km west of the first DOW7 deployment site (Figs. 2 and 4a) and arcs southwestward marks the rear-flank gust front. A slight wind shift from weak outbound velocities east of this line to weak inbound velocities west of it exists in the velocity data at 2245 UTC (Fig. 4b).

The low-level mesocyclone was most intense, as measured by the velocity difference across the radial velocity couplet, at approximately 2245 UTC (Fig. 4b). At this time, $\Delta v = 24$ m s^{-1} and the rotation was located near the back of the hook echo, about 17 km west of the radar site. This vortex was roughly 0.5 km in diameter and extended from the surface to an altitude of 450 m. By 2248 UTC, rotation was still evident in low-level scans from DOW7, and the vortex maintained its strength with $\Delta v = 22$ m s^{-1}. Data from DOW6 (which was 4 km south of DOW7; Fig. 2) from the same time reveal weaker rotation (not shown). This could be a result of small differences in both the radar calibration and siting.

By 2250 UTC, the hook echo was still well defined (Fig. 5a), but an overall decrease in reflectivity had occurred. The forward flank of the cell also appeared to have narrowed slightly by this time. It must be considered that this volume scan (Fig. 5) is from DOW6, whereas the 2245 (Fig. 4), 2309 (Fig. 6), and 2320 (Fig. 7) scans are from DOW7, which stopped scanning at 2247 UTC to follow the storm southeastward. DOW6 would continue scanning for approximately eight more minutes (until 2258 UTC) before also moving southeast.

The velocity field is considerably different by 2250 UTC (Fig. 5b). Strong surface divergence owing to the forward-flank and rear-flank downdrafts is apparent along the major axis of the echo. Near-surface wind speeds appear to have strengthened significantly, although it is very likely that at least some of this increase is attributable to the different radar. The rear-flank gust front sharpened and propagated eastward such that it was 5 km west of DOW6. The forward-flank gust front is also apparent near the southern edge of the forward-flank reflectivity core (Figs. 5a and 5b). A second line of enhanced reflectivities arcing west-northwestward from the tip of the hook echo could possibly be due to a secondary RFD surge (e.g., Marquis et al. 2008), although no significant wind shift exists in the velocity data to substantiate this thought.

By 2309 UTC, the reflectivity core and hook echo were largely unchanged from earlier volume scans (Fig. 6a). At this time, DOW7 was at its second deployment site, roughly 25 km SSE of its first site (Fig. 2). Additional convection that had formed to the rear of the storm began to near

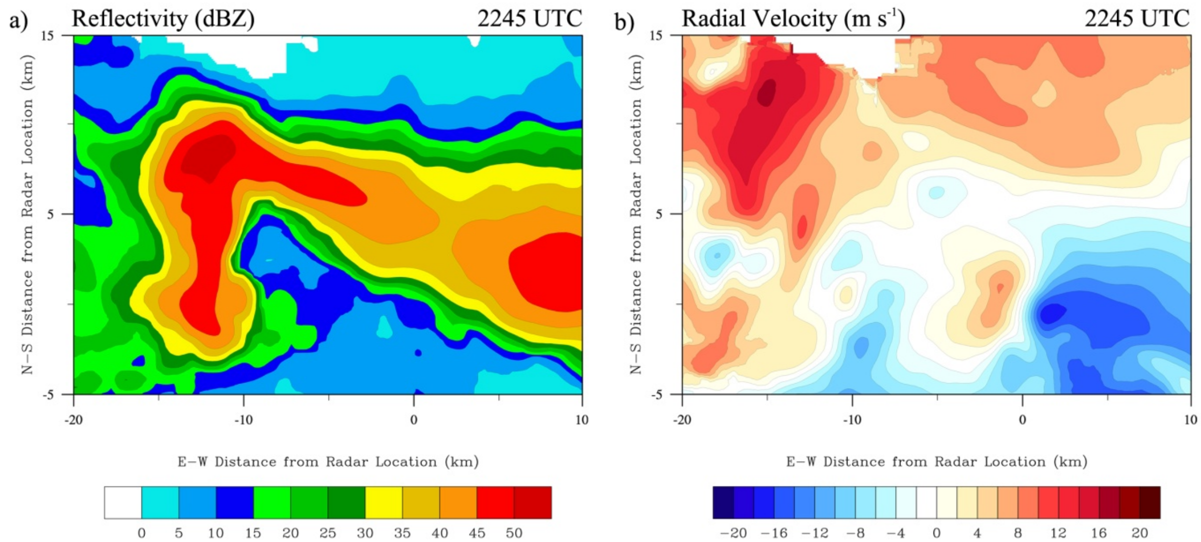

FIG. 4. Objectively analyzed (a) radar reflectivity (dBZ) and (b) radial velocity (m s^{-1}) from DOW7 at 2245 UTC 6 June 2010. Data are at 100 m above ground level (AGL).

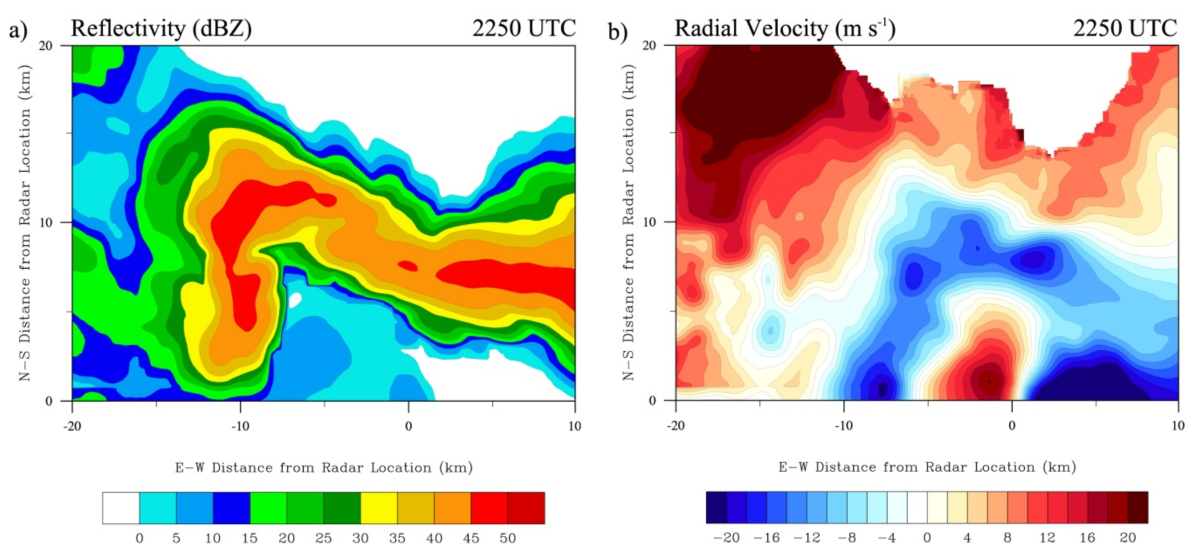

FIG. 5. Objectively analyzed (a) radar reflectivity (dBZ) and (b) radial velocity (m s^{-1}) from DOW6 at 2250 UTC 6 June 2010. Data are at 100 m AGL.

the supercell, and is visible as the band of high reflectivities extending northwestward from the hook echo. A fine line of enhanced reflectivities marks the location of the rear-flank gust front approximately 3 km west and 8 km north of the radar site and is oriented nearly parallel to, but about 5 km east of the hook echo. Note that the apparent break in the gust front approximately 4 km west and 6 km north of the radar site is caused by beam blockage owing to several buildings and large trees northwest of the radar location.

Inflow wind speeds were near 12 m s^{-1} at 2309 UTC (Fig. 6b), slightly weaker than those seen in the 2250 UTC scan from DOW6 (Fig. 5b), but stronger than the initial values from DOW7 at 2245 UTC (Fig. 4b). No low-level rotation was present at this time. It is likely that the shallow circulation seen at 2245 UTC (Fig. 4b) was unable to persist within the surging rear-flank outflow.

At 2320 UTC, the storm began to weaken significantly (Fig. 7a). By this time, only a few isolated areas of reflectivity greater than 50 dBZ remained, and reflectivities within the hook echo

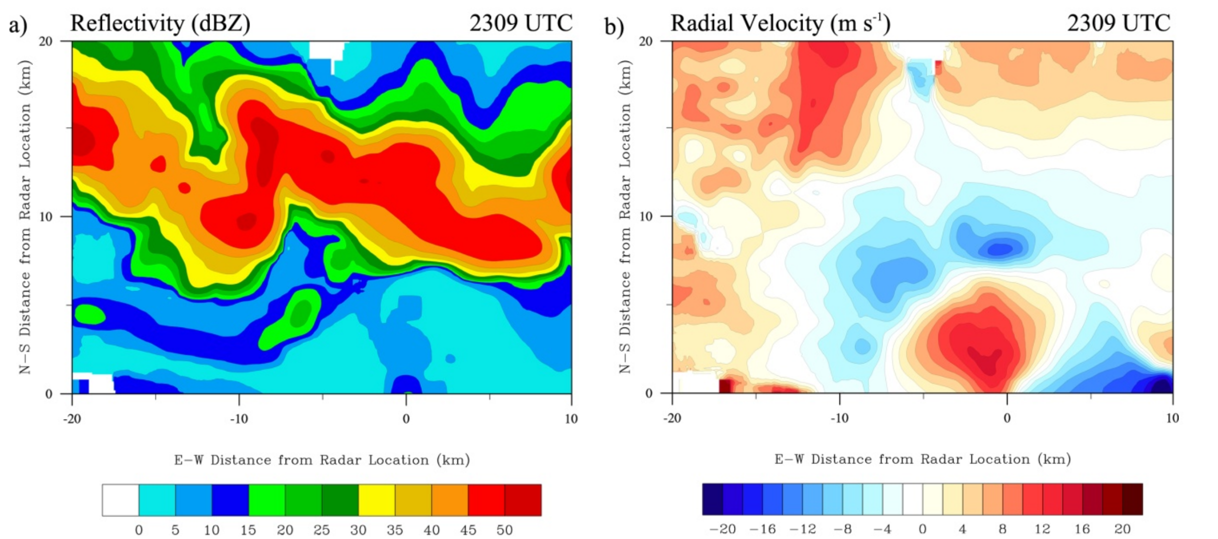

FIG. 6. Objectively analyzed (a) radar reflectivity (dBZ) and (b) radial velocity (m s^{-1}) from DOW7 at 2309 UTC 6 June 2010. Data are at 100 m AGL.

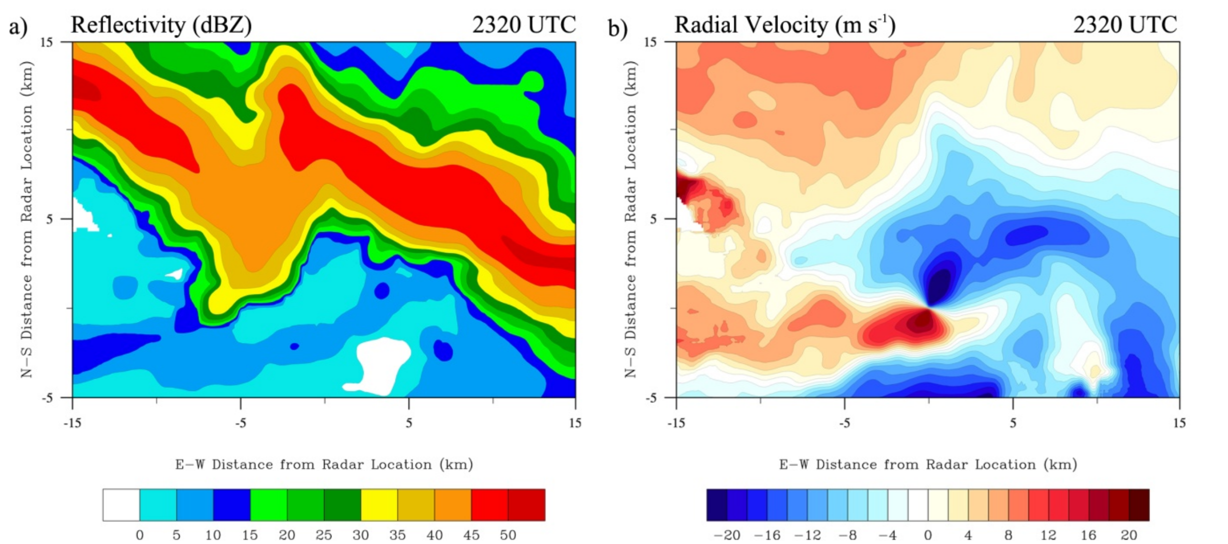

FIG. 7. Objectively analyzed (a) radar reflectivity (dBZ) and (b) radial velocity (m s^{-1}) from DOW7 at 2309 UTC 6 June 2010. Data are at 100 m AGL.

decreased to less than 45 dBZ. The hook echo also began to lose organization as seen by and the lack of an enhanced “ball-like” reflectivity signature near its southern tip. The rear-flank gust front continued to progress farther from the core of the storm, as it accelerated southeastward (and southeast of the radar location), reaching speeds in excess of 12 m s^{-1} (compare Figs. 6 and 7). By this time, it was located well ahead of the hook echo and continued to arc southwestward around the hook.

Whereas the wind shift at the gust front in at 2309 UTC was less evident (Fig. 6b), the 2320 UTC volume scan depicts a distinct wind shift at the gust front (Fig. 7b). Outbound velocities near 20 m s^{-1} behind the gust front converge with inbound velocities of approximately 16 m s^{-1} in the inflow region. As the advancing cold pool progressed farther southeast, the updraft became completely segregated from the warm moist inflow, forcing the storm to continue to weaken. At this time, DOW radars followed the storm, but as the weakening trend continued, they abandoned this storm for another storm to the north, which is not discussed in this paper.

4. Conclusions

The Doppler radar analyses of this nontornadic supercell presented herein indicate that this storm, which was initially a mature supercell with a low-level mesocyclone ($\Delta v = 24$ m s^{-1}), weakened as the rear-flank gust front advanced several kilometers in front of the hook echo and suspected updraft. The surging cold pool deprived the supercell updraft of the warm, moist air necessary for storm sustenance.

Further analysis utilizing dual-Doppler wind syntheses to diagnose three-dimensional flow, vorticity, and divergence fields near and within the storm will allow for additional conclusions to be drawn regarding the updraft strength, low-level trajectories, and vorticity budgets. Additionally, future work will entail the analysis of in-situ thermodynamic data obtained from mobile mesonets and sounding units to determine the relative buoyancy within the RFD (e.g., Markowski et al. 2002; Yaffe et al. 2012). It may also be beneficial in the future to examine NOAA X-Pol radar data to fill temporal voids in the DOW data, especially for the dual-Doppler wind syntheses. As we continue this research, we are hopeful that the analysis of this case, as well as the examination of additional data collected during VORTEX2 by others will allow for significant strides to be made in distinguishing between tornadic and nontornadic supercells.

Acknowledgements. We want to thank all of the VORTEX2 volunteers (too numerous to mention) who helped with the collection of data. We also wish to thank David Wojtowicz and Ken Patten of the Department of Atmospheric Sciences at the University of Illinois for computing assistance, Rachel Humphrey of the Center for Severe Weather Research for help obtaining the data, and Maxwell Smith and Tim Cermak for their help with graphics. Financial support from the Department of Atmospheric Sciences at the University of Illinois Urbana-Champaign is also acknowledged.

REFERENCES

Atkins, N. T., A. McGee, R. Ducharme, R. M. Wakimoto, and J. Wurman, 2012: The LaGrange tornado during VORTEX2. Part II: Photogrammetric analysis of the tornado combined with dual-Doppler radar data. *Mon. Wea. Rev.*, **140**, 2939–2958.

Barnes S. L., 1964: A technique for maximizing details in numerical weather map analysis. *J. Appl. Meteor.*, **3**, 396–409.

Beck, J. R., J. L. Schroeder, and J. M. Wurman, 2006: High-resolution dual-Doppler analyses of the 29 May 2001 Kress, Texas, cyclic supercell. *Mon. Wea. Rev.*, **134**, 3125–3148.

Frame, J., P. Markowski, Y. Richardson, J. Straka, and J. Wurman, 2009: Polarimetric and dual-Doppler radar observations of the Lipscomb County, Texas, supercell thunderstorm on 23 May 2002. *Mon. Wea. Rev.*, **137**, 544–561.

Kosiba, K., J. Wurman, Y. Richardson, P. Markowski, P. Robinson, and J. Marquis, 2012: Genesis of the Goshen County, Wyoming, tornado on 05 June 2009 during VORTEX2. *Mon.Wea. Rev.*, in press.

Kumjian, M. R. and A. D. Schenkman, 2008: Interpretation of the “flying eagle” radar signature in supercells. Preprints, *24th Conference on Severe Local Storms*, Amer. Meteor. Soc., Savannah, GA, paper P14.2

Markowski, P.M. , J. M. Straka, and E. N. Rasmussen, 2002: Direct surface thermodynamic observations within the rear-flank downdrafts of nontornadic and tornadic supercells. *Mon. Wea. Rev.*, **130**, 1692–1721.

Markowski, P., Y. Richardson, J. Marquis, J. Wurman, K. Kosiba, P. Robinson, D. Dowell, E. Rasmussen, and R. Davies-Jones, 2012: The pretornadic phase of the Goshen County, Wyoming, supercell of 5 June 2009 intercepted by VORTEX2. Part I: Evolution of kinematic and surface thermodynamic fields. *Mon. Wea. Rev.*, **140**, 2887-2915.

Markowski, P., Y. Richardson, J. Marquis, R. Davies-Jones, J. Wurman, K. Kosiba, P. Robinson, E. Rasmussen, and D. Dowell, 2012: The pretornadic phase of the Goshen County, Wyoming, supercell of 5 June 2009 intercepted by VORTEX2. Part II: Intensification of low-level rotation. *Mon. Wea. Rev.* **140**, 2916-2938.

Marquis, J., Y. P. Richardson, and J. M. Wurman, 2007: Kinematic observations of misocyclones along boundaries during IHOP. *Mon. Wea. Rev.*, **135**, 1749–1768.

Marquis, J., Y. Richardson, P. Markowski, D. Dowell, and J. Wurman, 2012: Tornado maintenance investigated with high-resolution dual-Doppler and EnKF analysis. *Mon. Wea. Rev.*, **140**, 3–27.

Oye, R., C. Mueller, and S. Smith, 1995: Software for radar data translation, visualization, editing, and interpolation. Preprints, *27th Conf. on Radar Meteorology*, Amer. Meteor. Soc., Vail, CO.

Oye, R. and M. Case, 1992: REORDER— A program for gridding radar data: Installation and use manual for the UNIX version. NCAR, 22 pp.

Pauley, P. M. and X. Wu, 1990: The theoretical, discrete, and actual response of the Barnes objective analysis scheme for one- and two-dimensional fields. *Mon. Wea. Rev.*, **118,** 1145–1164.

Trapp, R. J., 1999: Observations of nontornadic low-level mesocyclones and attendant tornadogenesis failure during VORTEX. *Mon. Wea. Rev.*, **127**, 1693–1705.

van den Broeke, M. S., J. M. Straka, and E. N. Rasmussen, 2008: Polarimetric radar observations at low levels during tornado life cycles in a small sample of classic Southern Plains supercells. *J. Appl. Meteor. and Climatology*, **47**, 1232-1247.

Wakimoto, R. M. and H. Cai, 2000: Analysis of a nontornadic storm during VORTEX 95. *Mon. Wea. Rev.*, **128**, 565–592.

Wakimoto, R. M., N. T. Atkins, and J. Wurman, 2011: The LaGrange tornado during VORTEX2. Part I: Photogrammetric analysis of the tornado combined with single-Doppler radar data. *Mon. Wea. Rev.*, **139**, 2233–2258.

Wurman, J., D. Dowell, Y. Richardson, P. Markowski, E. Rasmussen, D. Burgess, L. Wicker, and H. Bluestein, 2012: The second Verification of the Origins of Rotation in Tornadoes Experiment: VORTEX2. *Bull. Amer. Meteor. Soc.*, **93**, 1147–1170.

Wurman, J., J. Straka, E. Rasmussen, M. Randall, and A. Zahrai, 1997: Design and deployment of a portable, pencil-beam, pulsed, 3-cm Doppler radar. *J. Atmos. Oceanic Technol.*, **14**, 1502–1512.

Yaffe, K, A. Gordon, and J. Frame, 2012: Analysis of surface thermodynamic characteristics within the rear-flank downdraft of the Wichita, Kansas, tornadic supercell of 14 April 2012. Preprints, *26th Conf. on Severe Local Storms*, Amer. Meteor. Soc., Nashville, TN, paper P1.3.